NATIONAL ADVISORY COMMITTEE FOR AERONAUTICS

TECHNICAL NOTE 4194

COMPARISON OF HYDRODYNAMIC-IMPACT ACCELERATION AND RESPONSE FOR SYSTEMS WITH SINGLE AND WITH MULTIPLE ELASTIC MODES

By Robert W. Miller

Langley Aeronautical Laboratory
Langley Field, Va.

Washington

February 1958

NATIONAL ADVISORY COMMITTEE FOR AERONAUTICS

TECHNICAL NOTE 4194

COMPARISON OF HYDRODYNAMIC-IMPACT ACCELERATION AND RESPONSE FOR SYSTEMS WITH SINGLE AND WITH MULTIPLE ELASTIC MODES

By Robert W. Miller

SUMMARY

Hydrodynamic-impact tests were made with a multimode elastic model consisting of a rigid prismatic float and a flexible wing, and the results were compared with similar experimental results for a single-mode system and with theoretical solutions. The model had a ratio of sprung mass to hull mass of 0.48 and a first-mode natural frequency of 4.38 cycles per second. The tests were conducted in smooth water at fixed trims of 3° and 9° with flight-path angles of 14° and 6°, respectively, and over a range of velocity.

The analysis of the data and comparisons with other experimental and theoretical results indicated that the applied accelerations were in agreement with those obtained by the method of NACA Report 1074 and that the higher modes present in the multimode system had no significant effect on the applied accelerations.

INTRODUCTION

The development of large airplanes has caused the elastic behavior of airframe structures to become important. Considerable effort is being expended in attempts to evaluate the effects of this behavior on the externally applied dynamic loading of large airplanes during gusts, maneuvers, and landing impacts. In the case of water landings, this has reference to changes in the applied hydrodynamic force due to elastic action of the entire hull-wing structure and is not concerned with the high-frequency reactions of individual hull-bottom panels.

In reference 1, an analytical method for treating water landing of an elastic seaplane was presented in which interaction of the applied load and structural response was included, and it was shown that structural flexibility may have appreciable effects on the applied load. In reference 1, the elastic structure was represented by the assumption of a rigid prismatic float connected by a massless spring to a rigid upper

mass, and the solutions were based on hydrodynamic theory which had been experimentally confirmed for a rigid structure. Reference 2 substantiated these results by water-impact tests with an elastic model approximating the two-mass—spring system which consisted of a rigid prismatic float and a lightweight flexible wing supporting a concentrated mass on each tip.

The present tests made use of the model used in the investigation reported in reference 2, but the upper mass was distributed as uniformly as possible along the wing span instead of being concentrated at the tips. The purpose of testing this configuration was to determine the integrated influence of the higher modes of vibration present on the applied hydrodynamic loads and the validity of the two-mass-system approximation to the actual case where the masses are, in general, not concentrated on a weightless wing but distributed along the span.

SYMBOLS

a_n deflection coefficient for nth mode, function of time alone

C_l nondimensional acceleration coefficient, $\frac{n_l}{V_0^2}\left(\frac{g^2 W}{\rho}\right)^{1/3}$

C_t nondimensional time coefficient, $tV_0\left(\frac{\rho g}{W}\right)^{1/3}$

E Young's modulus of elasticity

F external applied load

f_n natural bending frequency

g acceleration due to gravity

I bending moment of inertia

M_n generalized mass of nth mode, $\int m w_n^2 dy$

m mass per unit span of wing

m_j mass at spanwise station j

m_L	lower, or hull, mass of two-mass system
m_S	upper, or sprung, mass of two-mass system
n_i	impact acceleration of center of gravity of vibrating system as free body, normal to surface, g units
t	time after initial contact
t_i	time between initial contact and maximum hydrodynamic force for structure considered rigid
t_n	time required for one-fourth cycle of natural vibration ($n = 1,2,\ldots$)
V_0	resultant velocity at instant of contact with water surface
W	weight of model
w	deflection of elastic axis of wing, positive upward
$w(0)$	deflection of elastic axis of wing at center line, positive upward
w_n	deflection of elastic axis in nth mode, given in terms of unit tip deflection
y	distance along wing measured from airplane plane of symmetry
β	angle of dead rise
γ_0	flight-path angle at contact
ρ	mass density of fluid
τ	angle of trim, angle of keel relative to water surface
φ_j	ratio of deflection of fundamental mode at station j to deflection at center line
ω_n	natural circular frequency of vibration of nth mode

A dot denotes the derivative with respect to time. Where units are not given, any consistent system of units may be used.

APPARATUS

Basin

A sketch giving the general arrangement of the Langley impact basin and equipment was presented in figure 1 of reference 2. Briefly, the operation of the equipment is as follows: The carriage, to which the model is attached by means of a parallelogram drop linkage, is catapulted at the desired horizontal velocity and then allowed to coast along the tank rails to the test section. At the test section, the drop linkage is released and the model, under the action of gravity, attains the required vertical velocity, at which time the lift engine applies to it an upward force which can be set to simulate any desired constant wing lift throughout the impact. A more detailed description of this Langley impact-basin equipment is given in reference 3.

Model

Photographs of the model in testing position are presented in figures 1 and 2. The same model was used in the present tests as in the tests described in reference 2. It consisted of a symmetrical flexible beam (the elastic wing) rigidly attached at its midspan to the vertical drop linkage and a float model rigidly mounted below it by means of a dynamometer truss. Unwanted oscillations during catapulting and dropping of the model were prevented by means of telescoping tubes (see fig. 1(a)) which were locked to link the wing tips rigidly to the float during these phases but were released immediately before water contact to permit the oscillations induced by the impact.

Instrumentation

The standard carriage instrumentation, described in reference 3, was used to measure time histories of the lift force and of the horizontal and vertical components of velocity and displacement. Time histories of vertical acceleration were measured by strain-gage accelerometers located on the boom. Other accelerometers were located on the wing at about the position of the center of gravity of the sprung mass and at the first-mode nodal point. A dynamometer truss mounted between the float and the wing was used to measure load normal to the keel. Strain gages on the wing and position recorders mounted on the telescoping tubes were used to check the symmetry of wing bending.

TEST PROCEDURE AND PRECISION OF DATA

Standard test procedure as described in reference 3 was used, and the tests were made in smooth water. Part of the tests were made at a trim of 3° and a flight-path angle of 14°. The resultant contact velocity for these runs was varied from 22 to 45 feet per second. This velocity range resulted in a range of period ratios t_n/t_i from 0.6 to 1.2, where t_n is the time required for 1/4 cycle of natural vibration in the fundamental mode f_n (see table I) and t_i is the time between initial contact and maximum hydrodynamic force for the structure considered rigid. The rest of the tests were made at a trim of 9° and a flight-path angle of approximately 6°. The velocity for these runs was varied from 25 to 86 feet per second to give a t_n/t_i range of 0.3 to 0.8. (See table II.)

The total dropping weight used was 2,400 pounds, the boom and float being loaded as lightly as possible and the remainder of the weight being distributed along the wing. The amount of weight apportioned to each mass and the resulting mass ratio of the system were determined by the following calculations: With the use of the actual mass distribution of the model (fig. 3(a)) and the known stiffness distribution of the wing, the fundamental free-free mode of the system was calculated by the method of reference 4. (The calculated modal characteristics of the model with the distributed mass are given in table I and fig. 4.) With this mode and mass distribution, the mass ratio of the equivalent two-mass—spring system was computed by means of the following equation, which is another form of equation (B6) of reference 1:

$$\frac{m_S}{m_L} = \frac{\Sigma m_j}{\Sigma m_j \varphi_j^2}$$

where m_j is the mass at a spanwise station j and φ_j is the ratio of the deflection of the fundamental mode at station j to the deflection at the center line. The mass ratio thus obtained was 0.48 instead of 0.60, the value which was used in reference 2. A few runs were made at the mass ratio of 0.48 with the sprung mass concentrated (figs. 2 and 3(b)) and with, as closely as possible, the same initial conditions of γ_0, τ, and V_0 in order to have direct experimental checks on the effect of mass distribution.

The apparatus and instrumentation used in the tests give measurements which are believed to be accurate within the following limits:

Horizontal velocity, ft/sec	±0.5
Vertical velocity, ft/sec	±0.2
Weight, lb	±2.0
Acceleration, g units	±0.2
Time, sec	±0.005
Vertical force, lb	±200.0

The curves of figure 5 are included as an indication of the consistency of the experimental data. Data are presented from three tests made at approximately the same initial conditions with the distributed upper mass loading. They show, for each run, the acceleration of the center of gravity of the vibrating system and the oscillatory acceleration of the hull or lower mass relative to the center of gravity. The center-of-gravity accelerations show a scatter of about 6 percent for the peak values and are in good agreement throughout the time histories. The hull oscillatory accelerations show more scatter of the peak values but are in fair agreement.

For one of the runs illustrated in figure 5 (run 14) a photographic copy of the original oscillograph record is presented in figure 6(a) in order to indicate the degree to which oscillations introduced by the higher modes of vibration are present. As a basis for comparison, a run having the concentrated loading and almost identical conditions (run 12) is presented in figure 6(b). The oscillations introduced by the higher mode appear most clearly on the normal-force and wing-acceleration traces.

ANALYSIS

An airframe, consisting of a hull and an elastic wing, undergoing a hydrodynamic impact can be considered as a free-free beam having an external force applied at its midpoint. The differential equation for wing bending, if damping is neglected, can then be written as

$$\frac{\partial^2}{\partial y^2} EI \frac{\partial^2 w}{\partial y^2} = -m\ddot{w} + \delta(y - 0)F \tag{1}$$

where w is the deflection of the elastic axis referred to a fixed reference plane, the term $\delta(y - 0)$ is the Dirac delta function applied at the center line of the model, and F is the external force.

The deflection of the system may be expressed in terms of the natural free-free modes:

$$w = a_0 + a_1 w_1 + a_2 w_2 + \cdots a_n w_n \tag{2}$$

where w_n is the deflection of the nth mode given in terms of unit tip deflection (fig. 4) and a_n is a function of time alone. In equation (2), a_0 denotes the free body vertical displacement of the model center of gravity, and a_1, a_2, . . . are the parts of the wing tip deflection associated with each mode.

The conditions for natural undamped vibration in any given mode are expressed by

$$\frac{\partial^2}{\partial y^2} EI \frac{\partial^2 w}{\partial y^2} = \omega_n{}^2 mw \tag{3}$$

where ω_n is the natural circular frequency of that mode. Combining equations (1) and (3) and introducing equation (2) yield

$$a_1\omega_1{}^2 mw_1 + a_2\omega_2{}^2 mw_2 = -m\left(\ddot{a}_0 + \ddot{a}_1 w_1 + \ddot{a}_2 w_2\right) + \delta(y - 0)F \tag{4}$$

where the assumption is made that only the first two modes of vibration are significant. If this equation is multiplied by w_n (where n is successively 1, 2, . . .) and then integrated over the wing (Galerkin procedure) and use is made of the orthogonality conditions $\left(\int mw_n\, dy = 0, \int my_m y_n\, dy = 0\right)$ then

$$M_0\ddot{a}_0 = F \tag{5a}$$

$$M_1\ddot{a}_1 + M_1\omega_1{}^2 a_1 = Fw_1(0) \tag{5b}$$

$$M_2\ddot{a}_2 + M_2\omega_2{}^2 a_2 = Fw_2(0) \tag{5c}$$

where for the rigid mode $w_n = w_0 = 1$ and $M_n = \int mw_n{}^2 dy$.

The quantity F which appears in equations (5) is the force defined by the hydrodynamic investigations of reference 5 (eq. (4)). It is of the form

$$F = A\left(3w^2\dot{w}^2 + w^3\ddot{w}\right) \tag{6}$$

The quantity A of equation (6) depends on the shape and attitude of that portion of the model in contact with the water.

Substituting, now, equations (2) and (6) into equations (5) and using the modal characteristics of the model (table I) lead to numerical solutions for the hydrodynamic force and wing bending moments. These solutions may be obtained by either matrix or iterative procedures.

Effectively, this procedure uses the known initial conditions to compute the loads and motions for the structure considered rigid. The loads are then applied to the elastic structure to obtain the structural response. With the addition of this response to the rigid-body motion, a new forcing function can be obtained which then includes a first approximation to the elastic effect. The procedure can then be iterated to obtain the desired degree of approximation in each mode.

As an aid in the estimation of elastic effects, the theoretical variation of the time histories of oscillatory acceleration of both center of gravity and hull with t_n/t_i are presented as three-dimensional plots in figures 7 and 8, respectively, for the mass ratios of 0.60 and 0.25 with initial conditions of 9° trim and 6° flight-path angle. Similar curves for four values of mass ratio with initial conditions of 3° trim and 14° flight-path angle are presented in reference 1. These curves may be used as references for observation of trends or they may be directly scaled for rough computation.

RESULTS AND DISCUSSION

In order to summarize the results, the test conditions, the peak theoretical and experimental accelerations, and the period ratios t_n/t_i are presented in table II. The test conditions are defined by the flight-path angle γ_0, the resultant velocity V_0, and the model trim angle at water contact τ. The experimental results presented in this table are the maximum values of the center-of-gravity accelerations of the vibrating system as a free body. The theoretical results are center-of-gravity accelerations of an elastic two-mass—spring system having the same mass and mass ratio and accelerations of a rigid body having the same total mass. Because of the lengthy calculations required for the theoretical solution of the elastic system, theoretical results for the elastic system were obtained for only 9 of the 32 runs.

The effect of the second mode on accelerations is shown in figure 9 for two representative cases. Solution for more than two modes was not considered necessary in this case, since the smallest readable vibrations during a run (see fig. 6(a)) exhibit a frequency of 20 to 28 cycles per

second, a frequency which compares well with the computed second-mode value (table I) of 24.4 cycles per second. In order to simplify the computations, solutions including the effects of one vibrational mode were obtained by use of the method described in reference 1 with the modifications of the constants as discussed in reference 2, which gives the same results as solutions of equations (5a) and (5b). The forcing function computed by this method was then used in equation (5c) as an initial forcing function, and an iterative process was used to compute a forcing function with the second-mode effect included.

Figure 9 presents the computed time histories of the accelerations of the center of gravity of the vibrating system, which are proportional to the external force on the system, and the hull oscillatory accelerations with respect to the center of gravity. It shows the comparison between the solution including the first mode and the solution including both the first and second modes. For a trim of 9° (fig. 9(a)) the effect of the second mode is quite small. For a trim of 3° (fig. 9(b)) the phasing of the second mode causes a delay in reaching maximum applied load but only a small change in its value. Thus, the computed effect of the second mode on the applied loads, as shown by the two cases investigated, appears to be of the order of 5 percent or less in maximum value.

For both conditions of trim and flight-path angle used during the tests, figure 10 again presents time histories of the oscillatory accelerations of the center of gravity and the hull; however, figure 10 compares the computed accelerations for a rigid body, the theoretical and experimental accelerations for a single-mode elastic body, and the experimental accelerations for a multimode elastic body. The rigid-body accelerations were obtained by use of the method of reference 6, and the theoretical elastic curves are the same as the single-mode curves in figure 9.

The plots of center-of-gravity acceleration in figure 10 show that the computed curves are a good approximation for the shape of the experimental time histories. The reduction of maximum load due to elasticity in the structure is also illustrated by comparison with the rigid-body curves. In figure 10(a) the peaks of the experimental accelerations agree with the peak of the computed curve within the range of experimental scatter of the data. In figure 10(b) the experimental curves agree well with each other but fall somewhat below the computed curve.

The computed curves of hull oscillatory acceleration of figure 10 appear to be a good approximation of the shape and frequency of the corresponding experimental curves but to exceed them in magnitude. Although it has not been definitely established, the discrepancy in magnitude may be due to structural and other forms of damping which are present in the experiment but not taken into account by the theory.

In all four plots of figure 10 the experimental acceleration curves for the distributed mass deviate from those for the concentrated mass by only a small amount. A small shift (well within the accuracy of the instrumentation) would cause the distributed-mass curve to oscillate about the concentrated-mass curve with approximately the same amplitude and frequency as the oscillation of the curve including the second mode about the curve including only the first mode in figure 9 for the corresponding cases. Thus, the second mode appears to have a definable effect, but this effect does not appreciably change the results obtained from those for a two-mass or single-mode system. It is possible that a three-mass system could be designed in which an accentuated second mode would have to be considered; however, for uniformly distributed loadings, taking into account a single elastic mode appears to be adequate.

Figure 11 presents the ratio of elastic-body acceleration to rigid-body acceleration as a function of the ratio of the first natural period of the system to the impact period. The data for a mass ratio of 0.48, which are presented in table II, show a comparison of the maximum experimental accelerations for both the distributed and the concentrated loadings with maximum accelerations computed by use of the theory of reference 1. A similar comparison, but for concentrated loading only, is shown in the plots for a mass ratio of 0.60, which use the data from table I of reference 2. Comparison with maximum accelerations computed by use of the rigid-body theory of reference 6 for the same initial conditions is shown by the deviation of the plotted points from the value of unity indicated by the dashed line.

The experimental elastic-body acceleration data, for a mass ratio of 0.48, contain results for both distributed and concentrated upper-mass loadings, and the concentrated-load points appear to lie within the scatter of the distributed-load points. Thus, the method for determining the two-mass system equivalent to a given distributed-mass system as described in reference 1 is seen to produce similar results for the cases for which, the initial conditions being similar, a direct comparison is possible.

The comparisons of the theoretical and experimental maximum accelerations for an elastic body demonstrate that the theory gives a good approximation of the experimental results for both trim and flight-path angles at a mass ratio of 0.60 and for a trim of 9° and a flight-path angle of 6° at a mass ratio of 0.48. For these conditions, the theoretical points lie, generally, within the scatter of the experimental points. For a trim of 3° and a flight-path angle of 14°, at a mass ratio of 0.48, the experimental data lie somewhat below the theoretical data. This discrepancy could have been caused by hydrodynamic conditions not taken into account by the present theory such as bow or chine immersion.

As was indicated in reference 1, the comparisons between elastic-body and rigid-body accelerations show that the elastic-body results can be as much as 30 percent lower than those of a rigid body at the same initial conditions of impact. For ranges of mass ratio and period ratio other than those presented, which are within the practical range, the reduction of maximum acceleration due to elasticity of the body can be greater than the 30-percent reduction obtained herein or the elastic-body acceleration can actually exceed that of the rigid body.

CONCLUSIONS

Comparisons of experimental data obtained in hydrodynamic impacts of a multimode elastic model consisting of a rigid prismatic float and a flexible wing with the theoretical and experimental results for a single-mode system having the same mass ratio have led to the following conclusions:

1. The theoretical center-of-gravity accelerations computed by the methods of NACA Report 1074 are generally in agreement with the experimental results within the range of scatter of the data.

2. The higher modes present in the elastic system had no significant effect on the center-of-gravity accelerations.

3. Curves of the theoretical oscillatory accelerations of the hull approximated the shape of the curves of the experimental results but overestimated their magnitude, probably because of damping in the system.

Langley Aeronautical Laboratory,
National Advisory Committee for Aeronautics,
Langley Field, Va., October 16, 1957.

REFERENCES

1. Mayo, Wilbur L.: Hydrodynamic Impact of a System With a Single Elastic Mode. I - Theory and Generalized Solution With an Application to an Elastic Airframe. NACA Rep. 1074, 1952. (Supersedes NACA TN 1398.)

2. Miller, Robert W., and Merten, Kenneth F.: Hydrodynamic Impact of a System With a Single Elastic Mode. II - Comparison of Experimental Force and Response With Theory. NACA Rep. 1075, 1952. (Supersedes NACA TN 2343.)

3. Batterson, Sidney A.: The NACA Impact Basin and Water Landing Tests of a Float Model at Various Velocities and Weights. NACA Rep. 795, 1944. (Supersedes NACA WR L-163.)

4. Houbolt, John C., and Anderson, Roger A.: Calculation of Uncoupled Modes and Frequencies in Bending or Torsion of Nonuniform Beams. NACA TN 1522, 1948.

5. Milwitzky, Benjamin: Generalized Theory for Seaplane Impact. NACA Rep. 1103, 1952.

6. Mayo, Wilbur L.: Theoretical and Experimental Dynamic Loads for a Prismatic Float Having an Angle of Dead Rise of $22\frac{1}{2}^{\circ}$. NACA WR L-70, 1945. (Formerly NACA RB L5F15.)

TABLE I

MODAL CHARACTERISTICS OF MODEL

Mode	M_n, slugs	ω_n, radians/sec	f_n, cps	w(0)
Rigid	74.53	------	-----	1.000
1st	5.19	27.54	4.38	-.259
2d	4.91	153.49	24.4	.200

TABLE II

TEST DATA AND THEORETICAL PEAK VALUES FOR HYDRODYNAMIC IMPACT OF A MULTIMODE SYSTEM WITH MASS RATIO OF 0.48

Run	Initial conditions		Period ratio, $\frac{t_n}{t_i}$	Rigid body	Elastic body		Weight distribution
				Theoretical	Theoretical	Experimental	
	V_0, ft/sec	γ_0, deg		$n_{i,max}$, g	$n_{i,max}$, g	$n_{i,max}$, g	(a)
$\tau = 3^\circ$							
1	21.97	14.42	0.60	0.91	0.82	0.64	D
2	22.75	15.00	.63	1.00		.82	D
3	23.97	15.26	.68	1.20		.80	D
4	26.50	13.00	.66	1.11		.85	D
5	27.91	14.38	.76	1.46	1.25	.88	D
6	31.58	13.33	.80	1.65		1.12	D
7	31.96	14.44	.88	1.94		1.19	D
8	32.20	13.95	.84	1.85	1.56	1.11	D
9	32.33	14.79	.90	2.08		1.33	D
10	34.25	15.01	.95	2.40		1.65	C
11	34.66	14.47	.95	2.29		1.52	C
12	34.77	14.18	.94	2.22		1.52	C
13	34.84	14.63	.95	2.37		1.62	C
14	36.36	14.46	1.00	2.52	2.08	1.58	D
15	37.56	14.53	1.03	2.71		1.72	D
16	38.67	14.10	1.03	2.72		1.73	D
17	45.31	13.80	1.17	3.61	2.95	2.30	D
$\tau = 9^\circ$							
18	24.73	8.37	0.31	0.53		0.39	D
19	34.09	5.02	.30	.51		.48	D
20	53.81	6.73	.58	1.84		1.53	D
21	55.21	5.55	.51	1.51	1.34	1.20	D
22	65.49	6.07	.66	2.37	2.03	2.22	D
23	66.98	5.52	.63	2.23		1.78	D
24	75.38	5.75	.73	2.93		2.47	C
25	75.39	5.80	.74	3.03		2.57	C
26	76.14	5.74	.74	2.99		2.52	C
27	76.21	5.74	.74	2.99		2.66	C
28	76.34	5.78	.75	3.06	2.56	2.54	D
29	76.37	5.47	.72	2.79		2.40	D
30	76.81	5.39	.71	2.82		2.31	D
31	81.28	5.38	.75	3.16		2.55	D
32	85.64	5.62	.81	3.71	3.07	2.85	D

[a]D, distributed upper mass; C, concentrated upper mass.

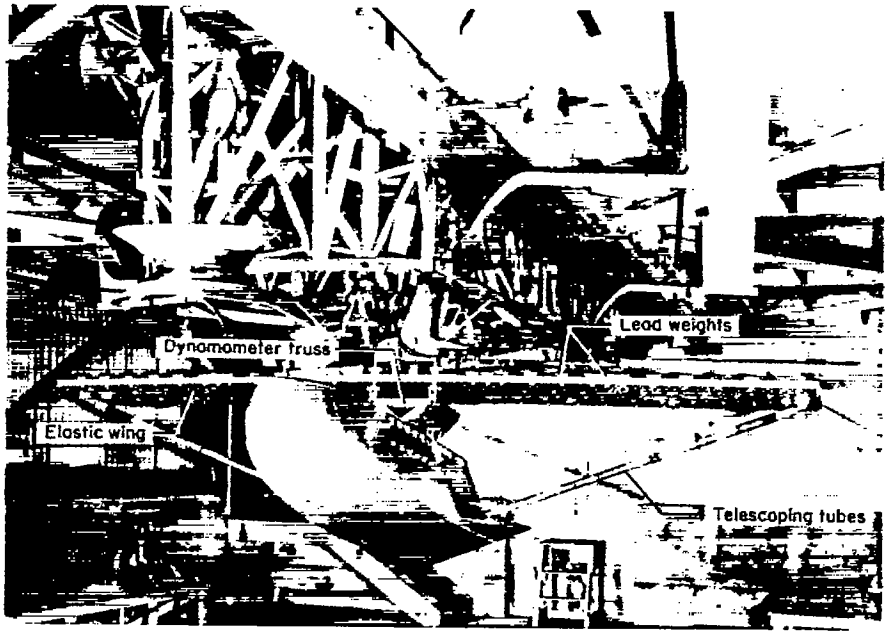

(a) One-quarter front view.

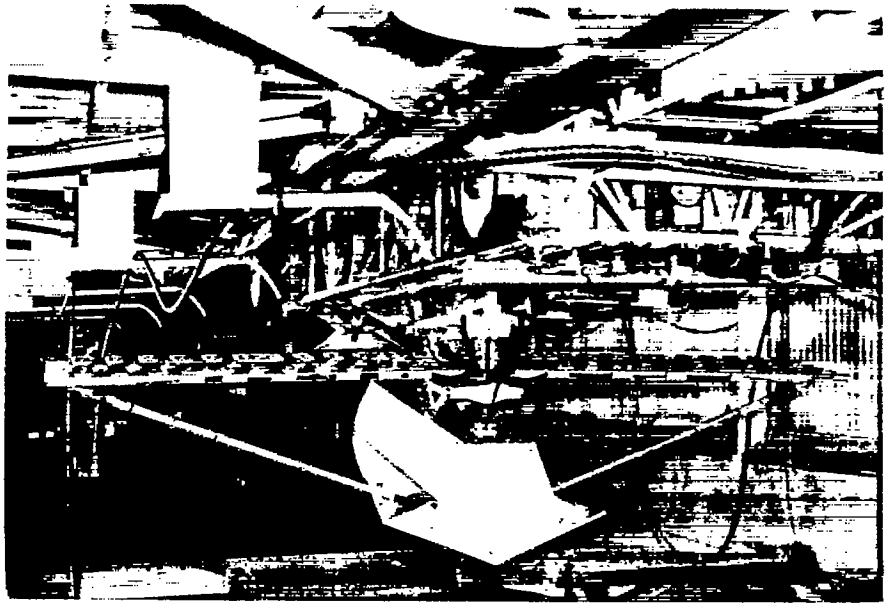

(b) One-quarter rear view. L-57-2796

Figure 1.- Views of model with distributed load. $m_S/m_L = 0.48$.

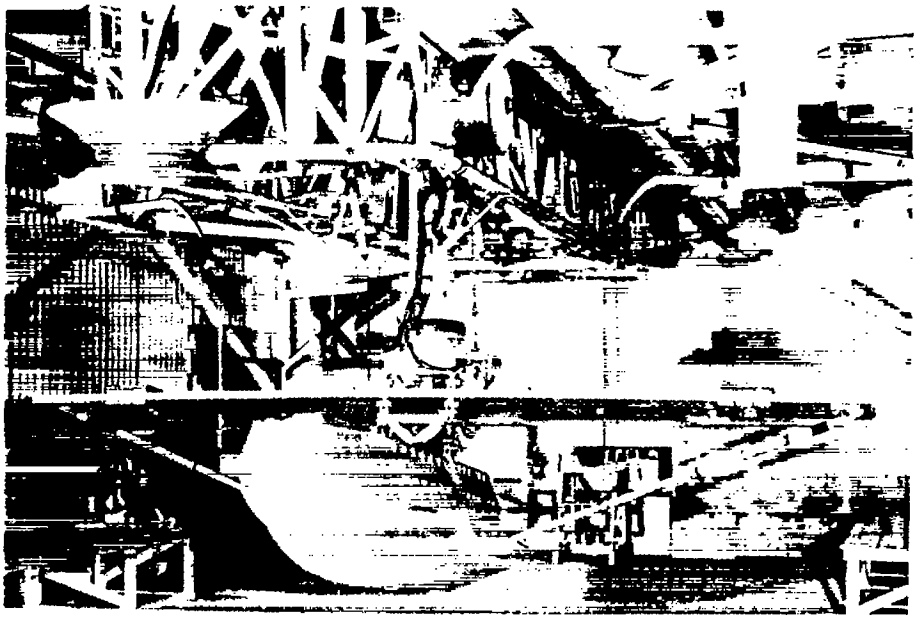

(a) One-quarter front view. L-63948

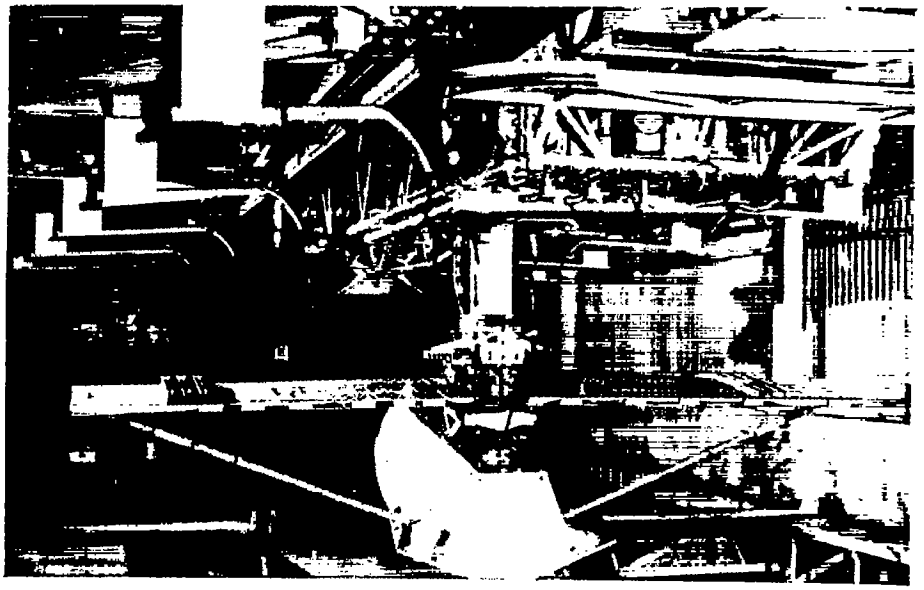

(b) One-quarter rear view. L-63950

Figure 2.- Views of model with concentrated load. $m_S/m_L = 0.48$.

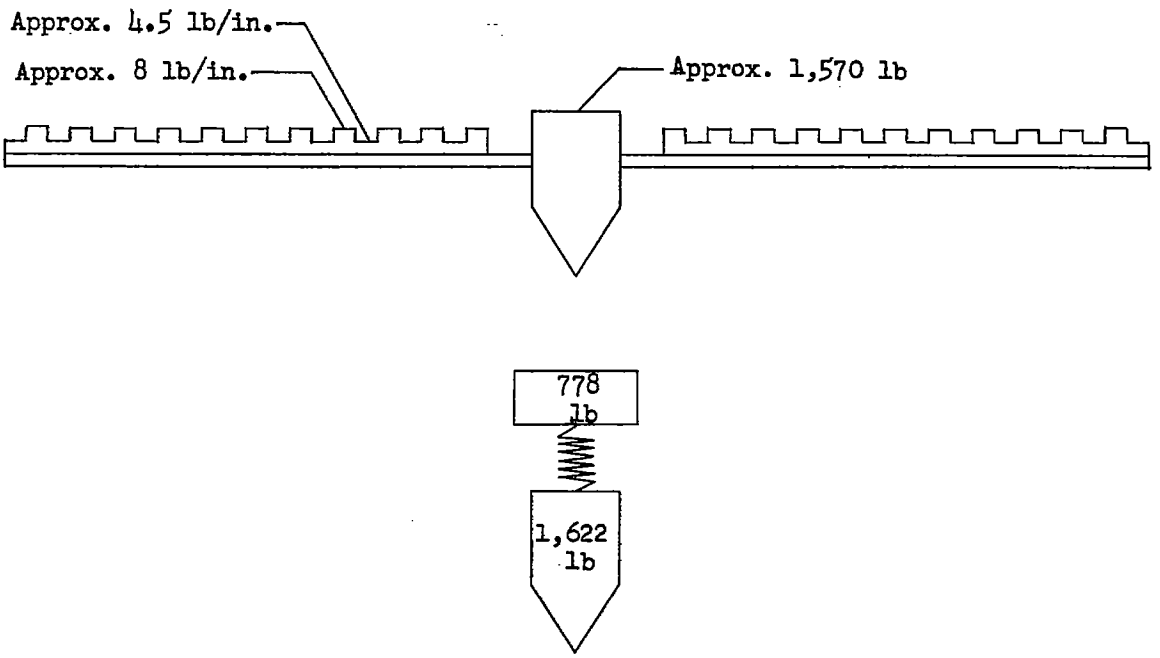

(a) Distributed load.

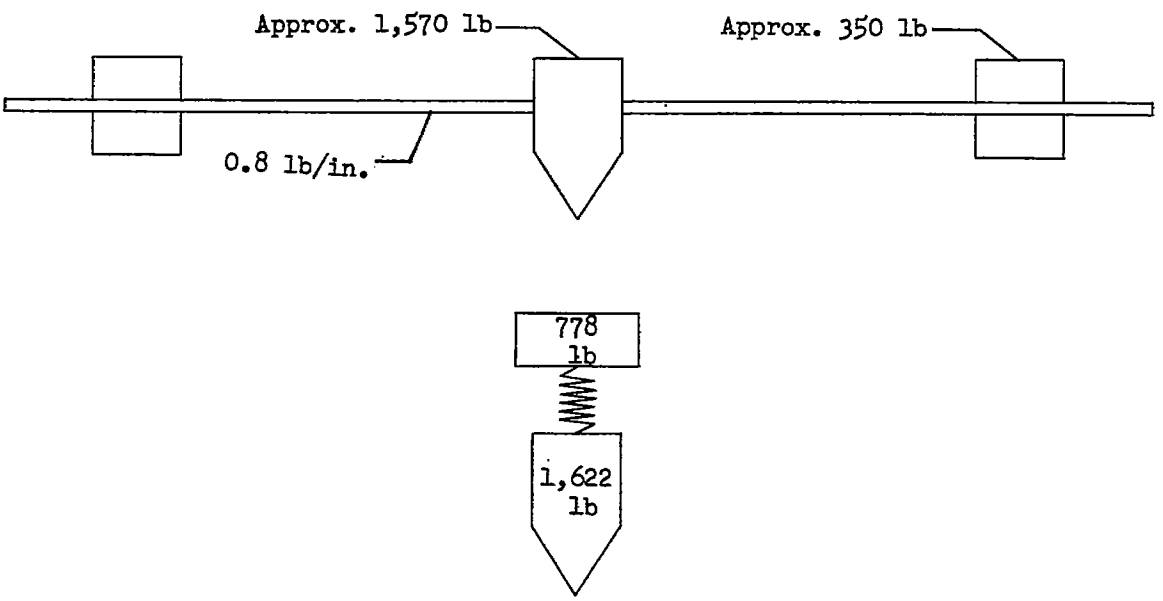

(b) Concentrated load.

Figure 3.- Schematic diagram of model.

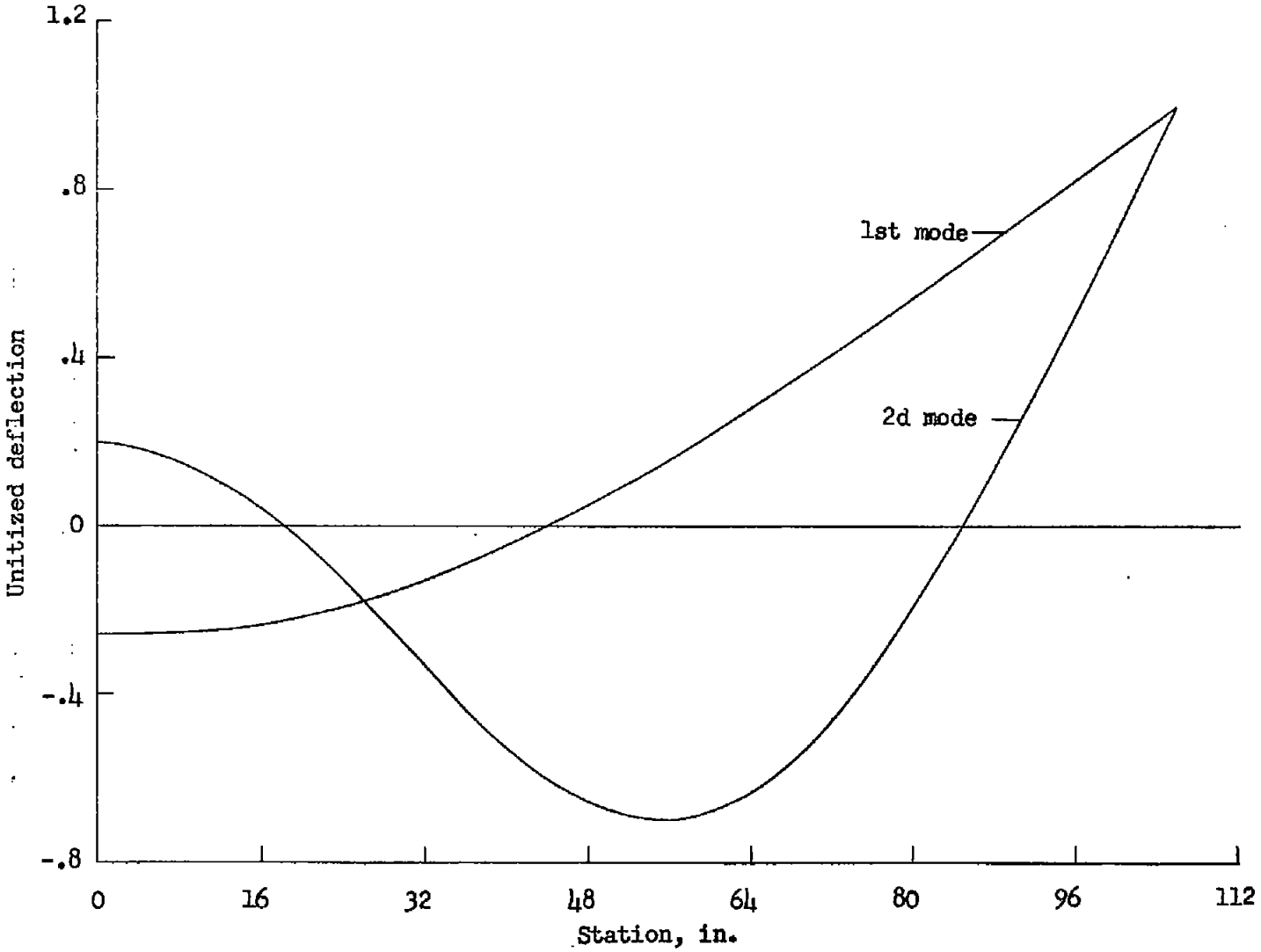

Figure 4.- Symmetrical bending mode shapes.

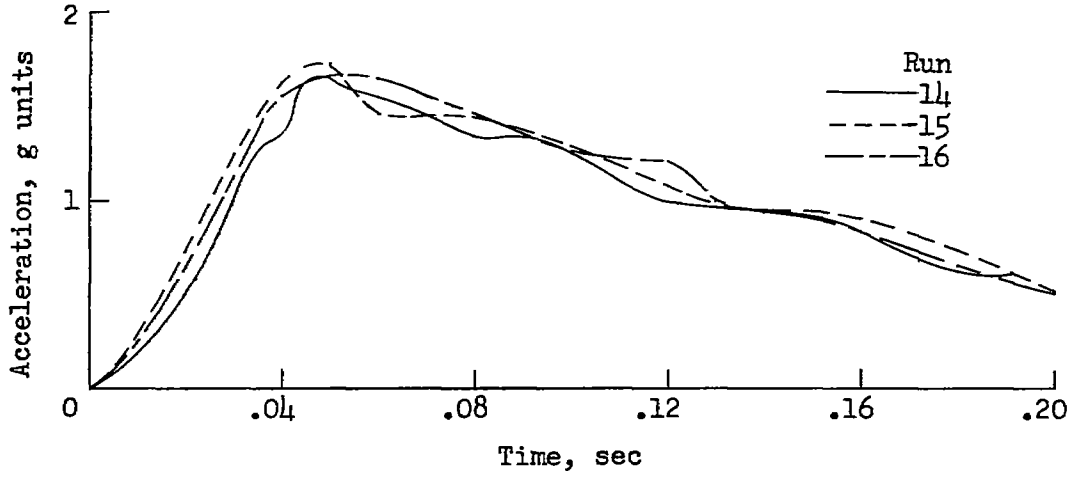

(a) Center-of-gravity acceleration.

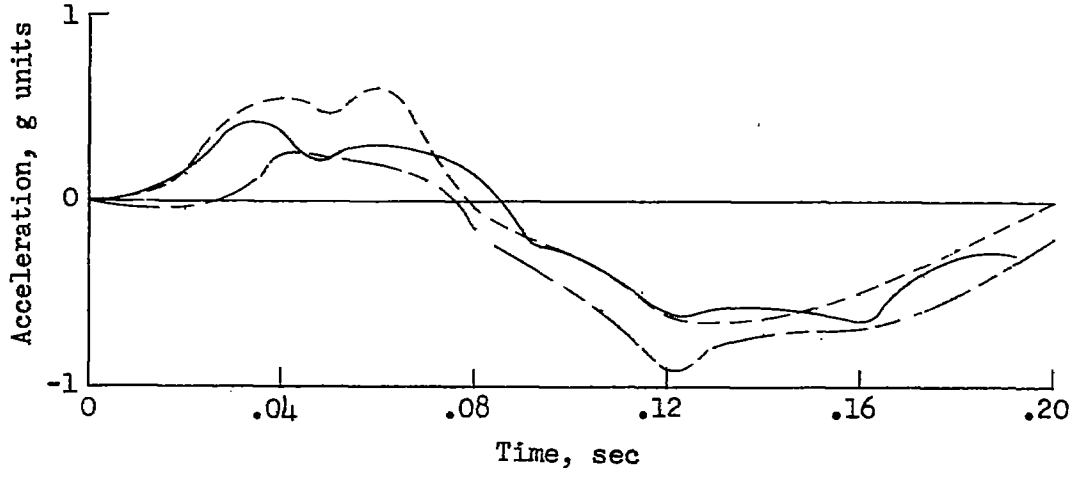

(b) Hull oscillatory (hull minus center of gravity) acceleration.

Figure 5.- Curves showing consistency of experimental data for model with distributed load.

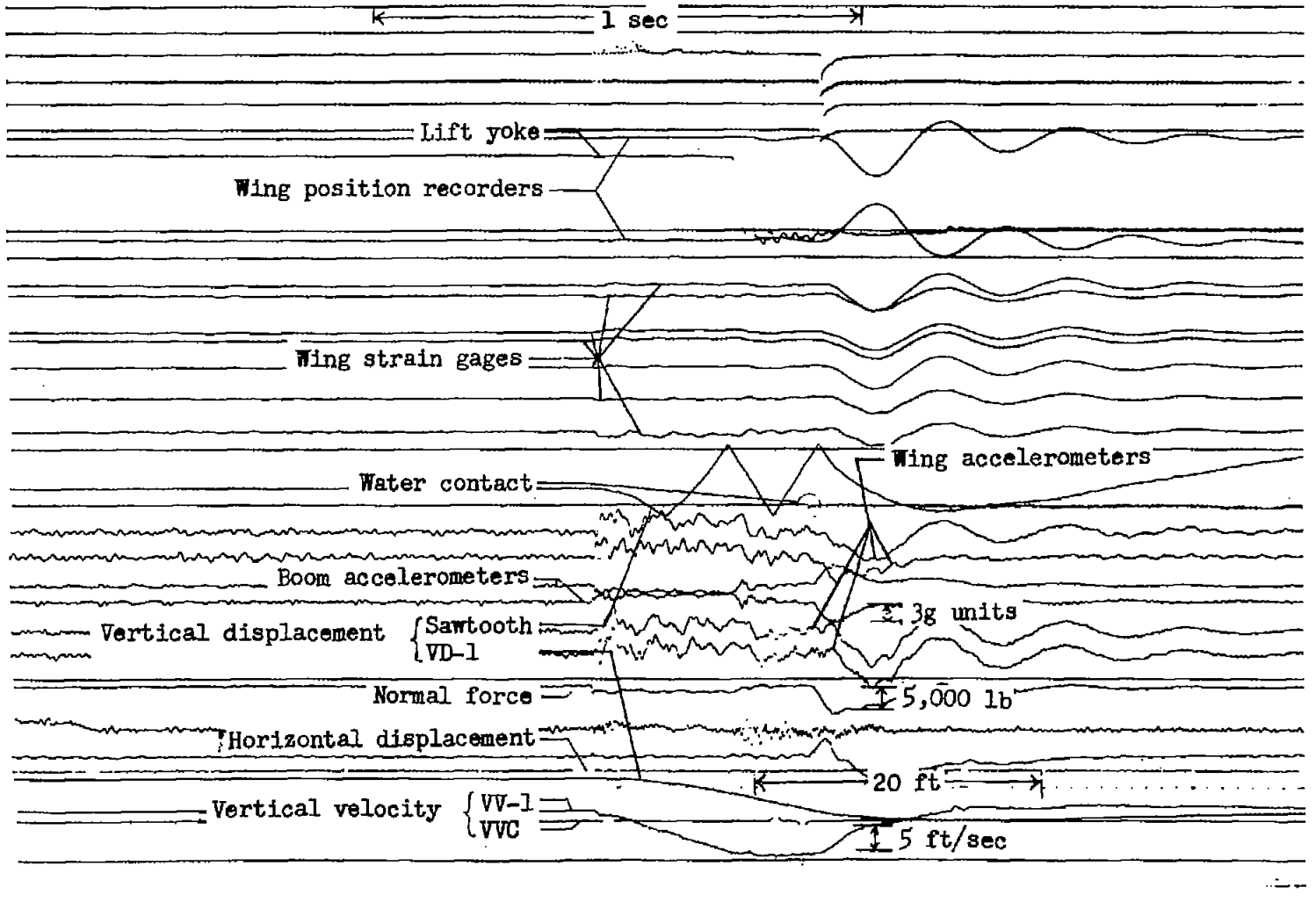

(a) Run 14; distributed loading.

Figure 6.- Typical oscillograph record obtained from tests having $\tau = 3^{\circ}$; $\gamma \approx 14^{\circ}$.

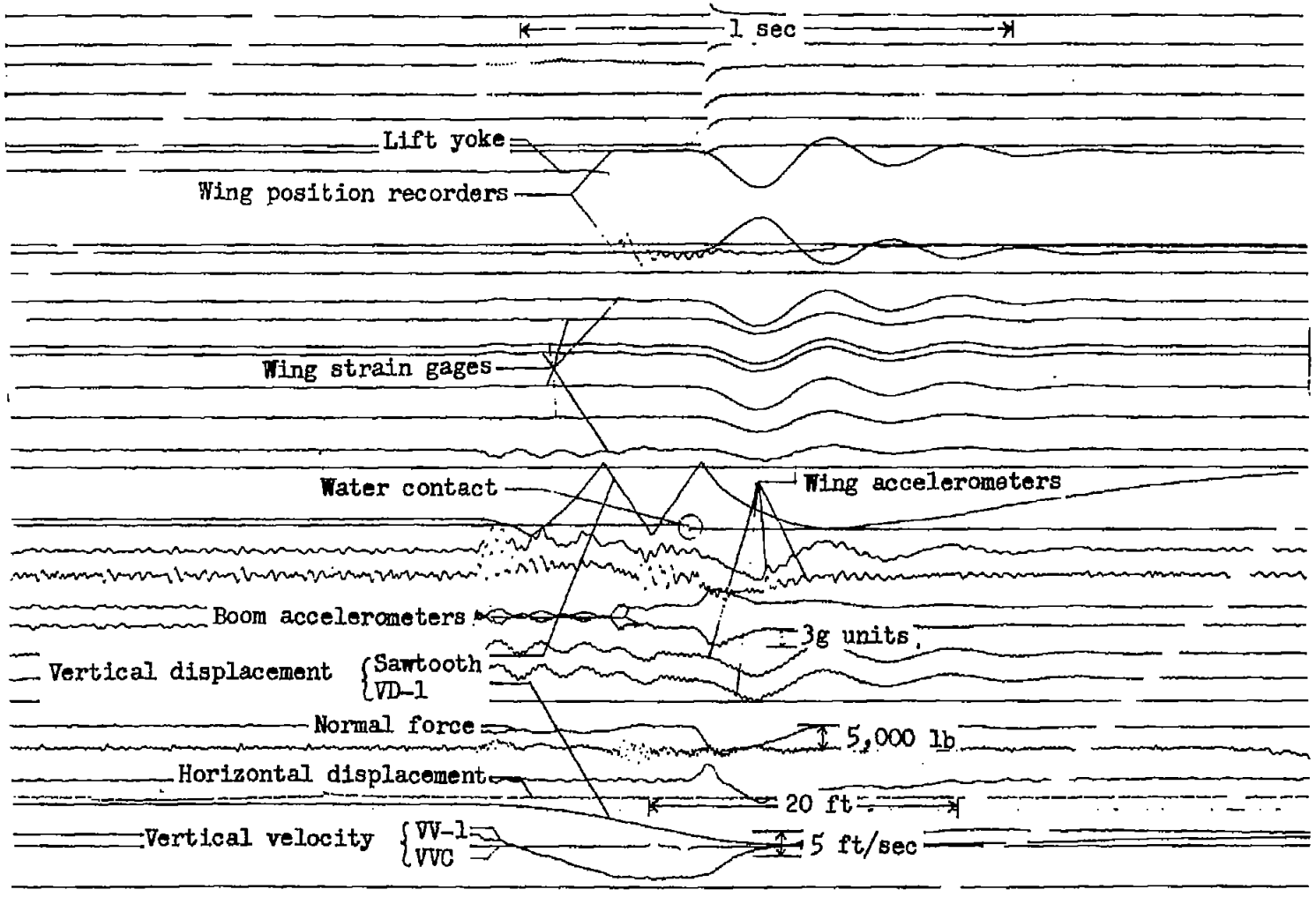

(b) Run 12; concentrated loading.

Figure 6.- Concluded.

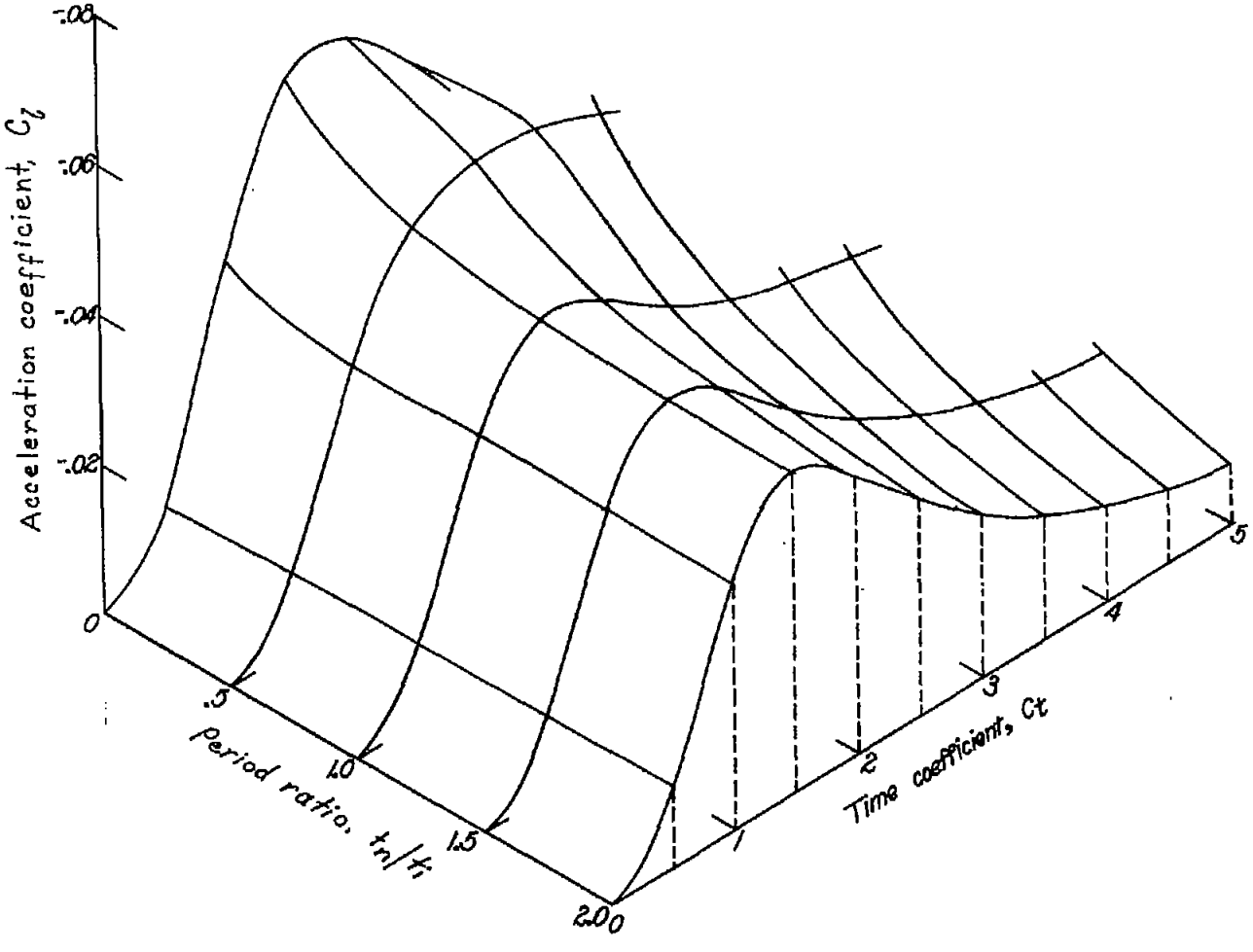

(a) $m_S/m_L = 0.60$; $\beta = 22\frac{1}{2}^\circ$; $\tau = 9^\circ$; $\gamma = 6^\circ$.

Figure 7.- Variation of center-of-gravity-acceleration coefficient with period ratio.

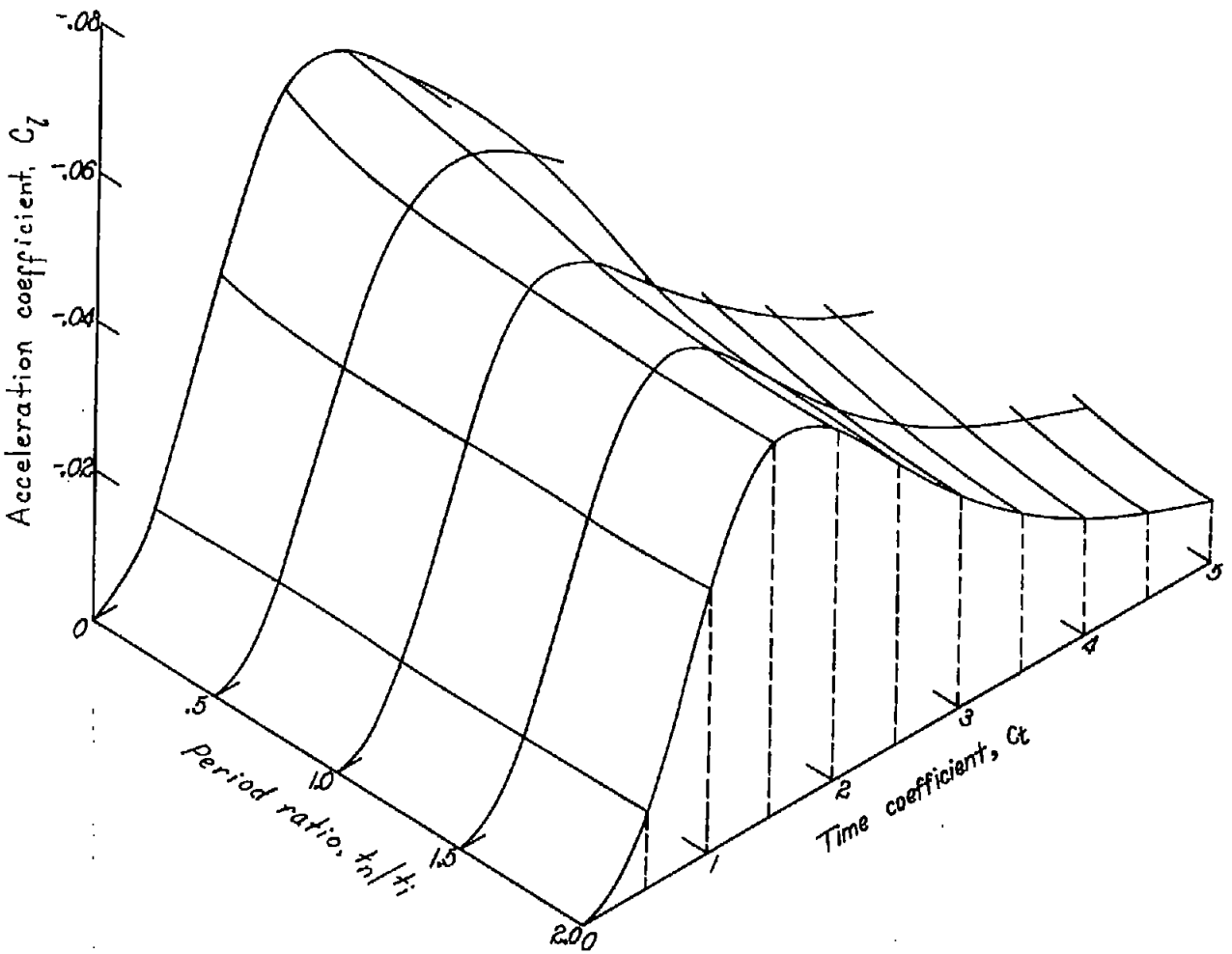

(b) $m_S/m_L = 0.25$; $\beta = 22\frac{1}{2}^\circ$; $\tau = 9^\circ$; $\gamma = 6^\circ$.

Figure 7.- Concluded.

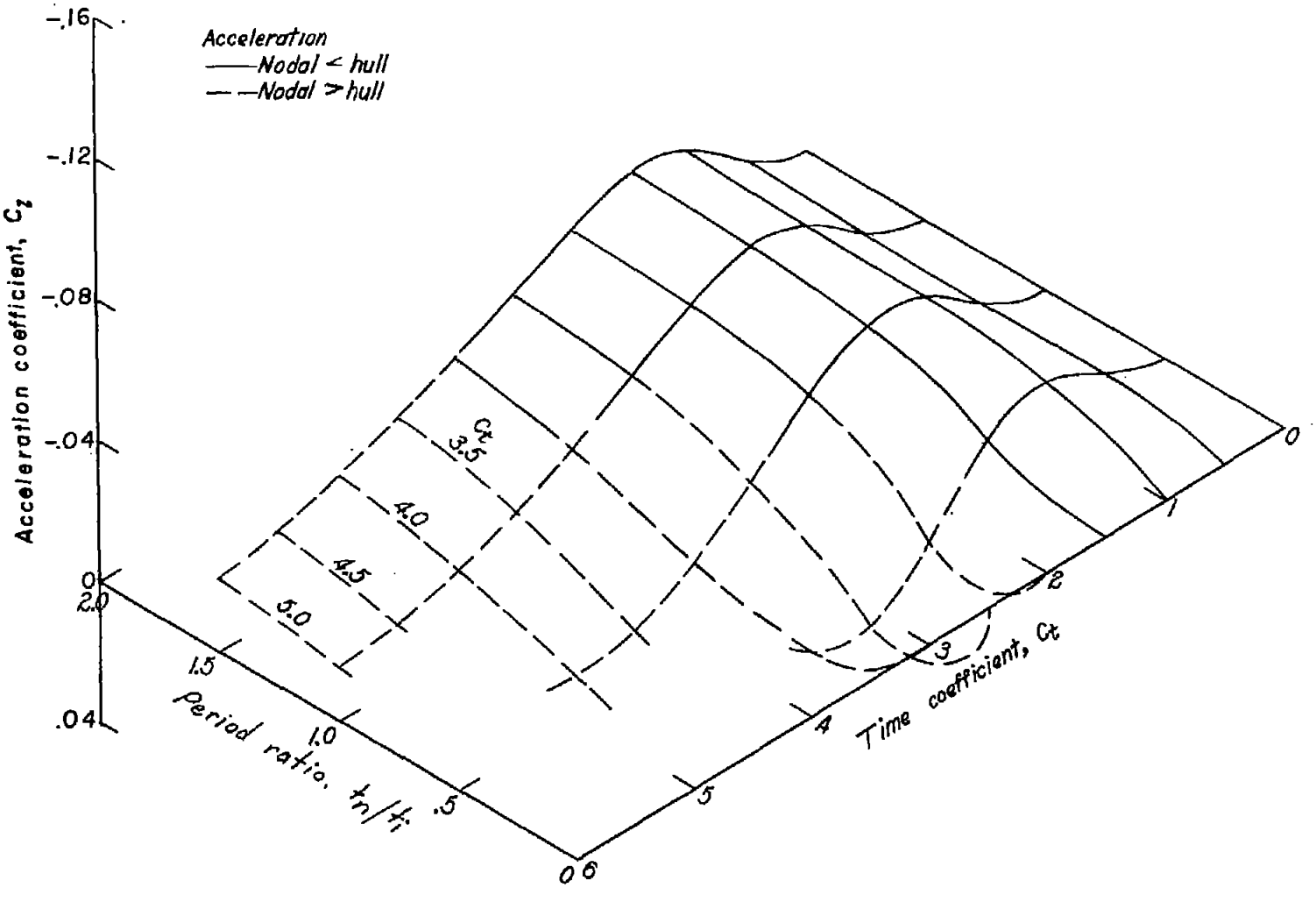

(a) $m_S/m_L = 0.60$; $\beta = 22\frac{1}{2}^\circ$; $\tau = 9^\circ$; $\gamma = 6^\circ$.

Figure 8.- Variation of oscillatory-acceleration coefficient with period ratio.

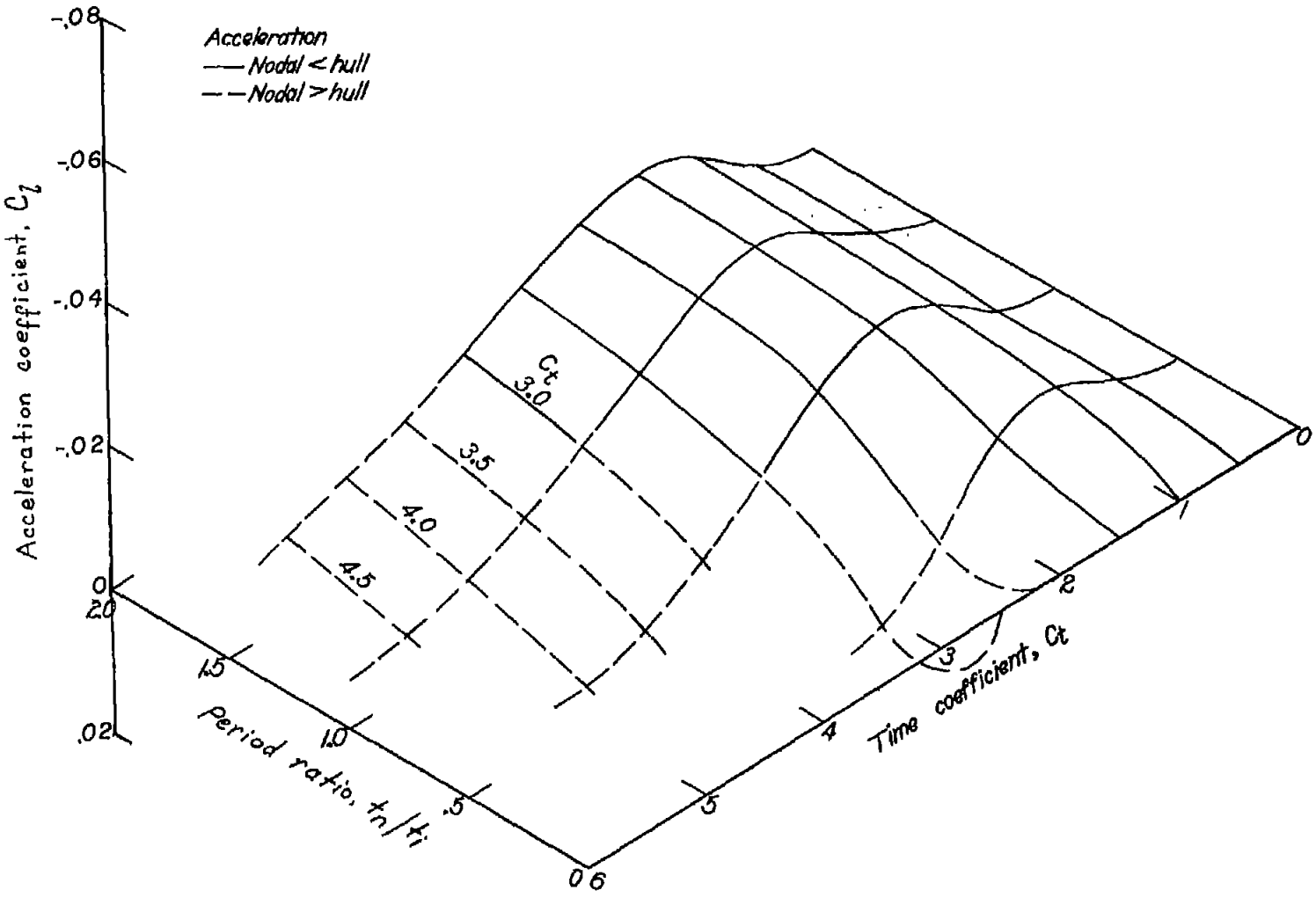

(b) $m_S/m_L = 0.25$; $\beta = 22\frac{1}{2}^\circ$; $\tau = 9^\circ$; $\gamma = 6^\circ$.

Figure 8.- Concluded.

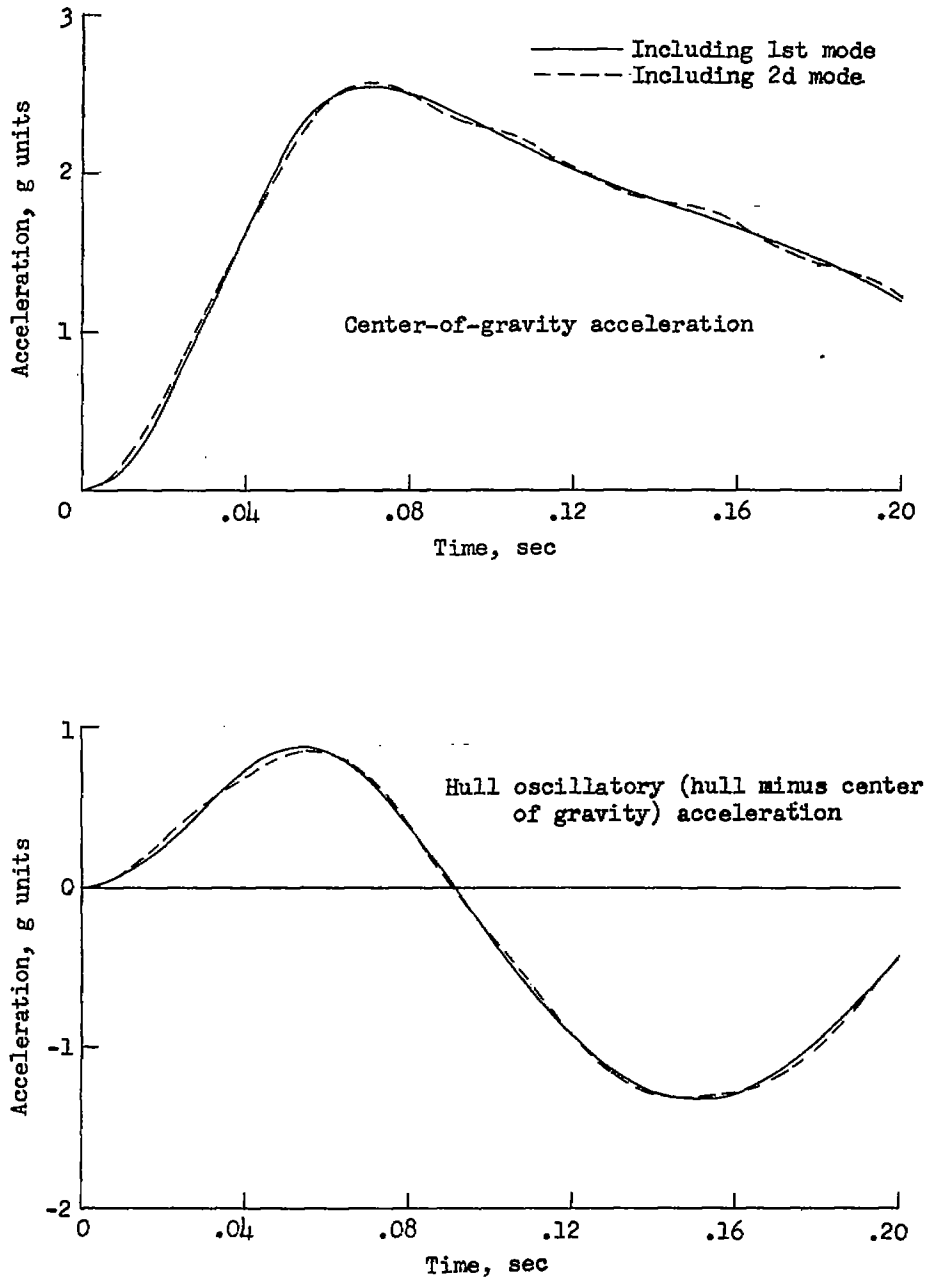

(a) Conditions of run 28; $\tau = 9^{\circ}$; $\gamma \approx 6^{\circ}$.

Figure 9.- Computed time histories showing influence of second mode.

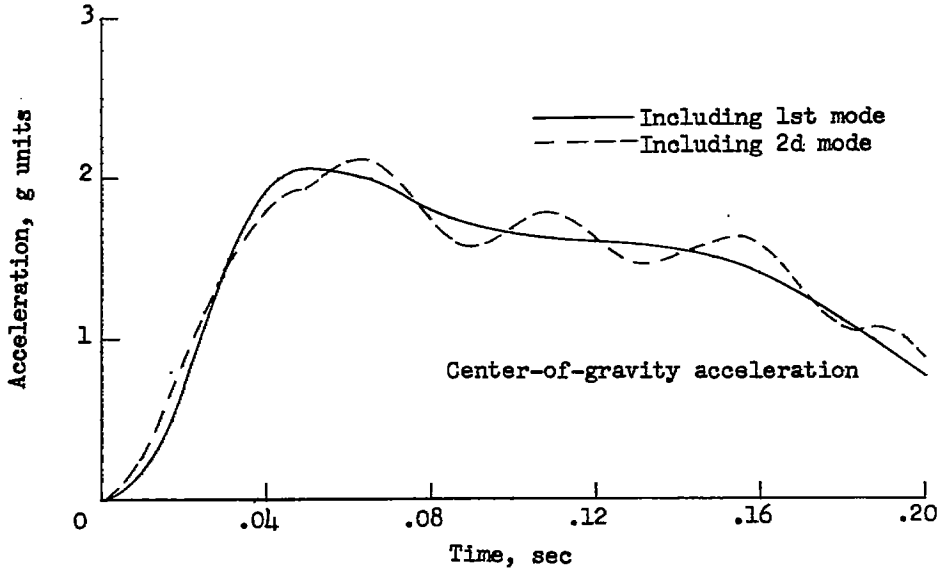

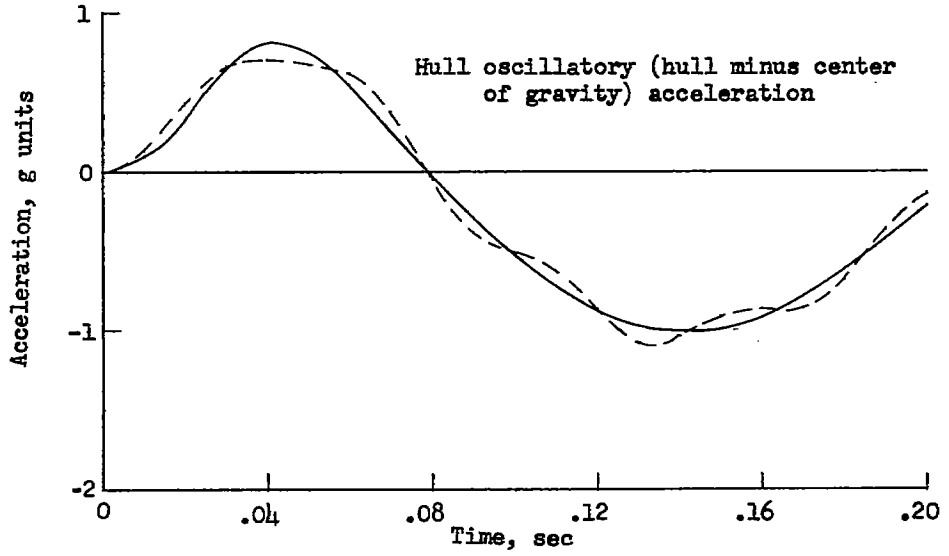

(b) Conditions of run 14; $\tau = 3^{\circ}$; $\gamma \approx 14^{\circ}$.

Figure 9.- Concluded.

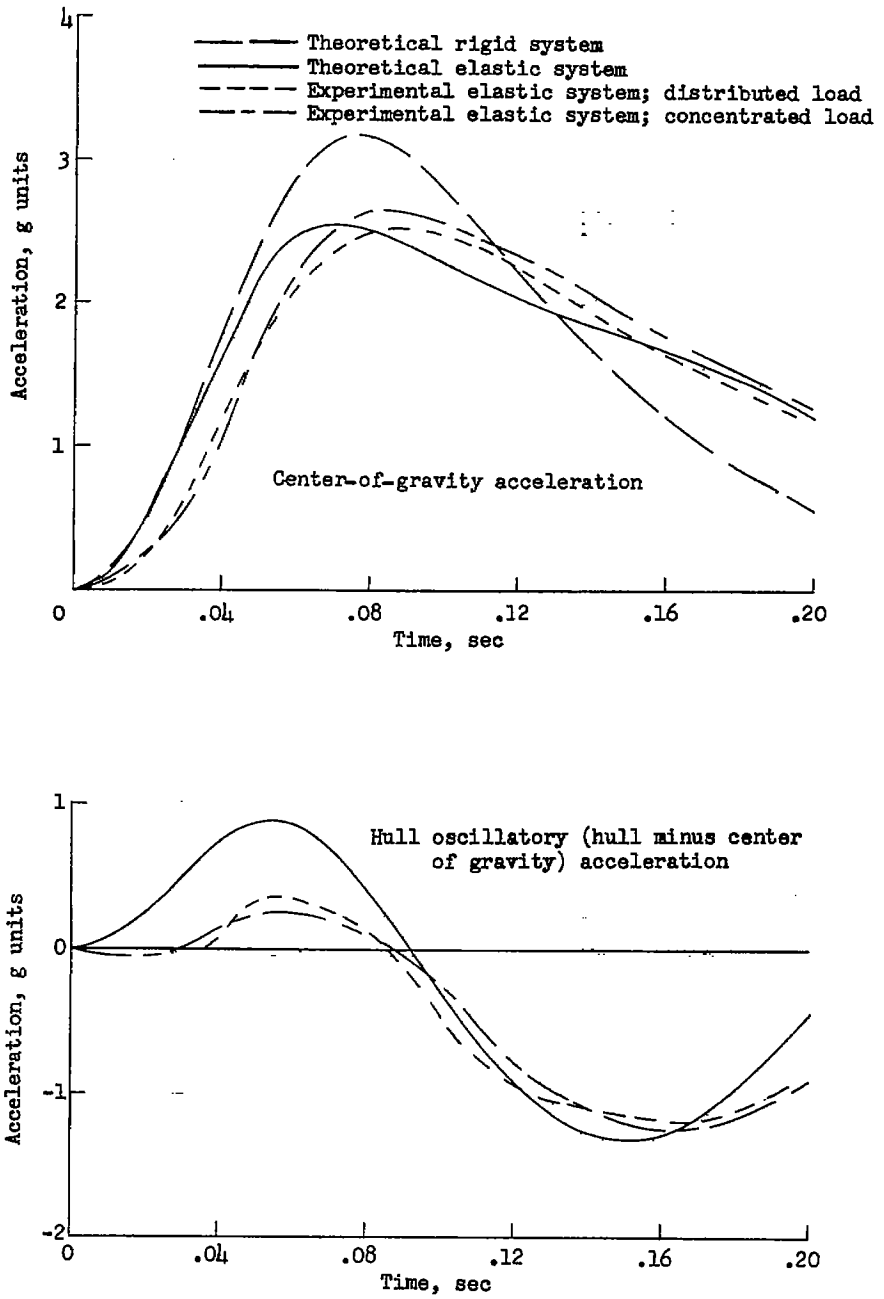

(a) Runs 27 and 28: $\tau = 9^{\circ}$; $\gamma \approx 6^{\circ}$; $V_0 \approx 76$ feet per second.

Figure 10.- Time-history comparison of theoretical and experimental hydrodynamic-impact acceleration for a two-mass system.

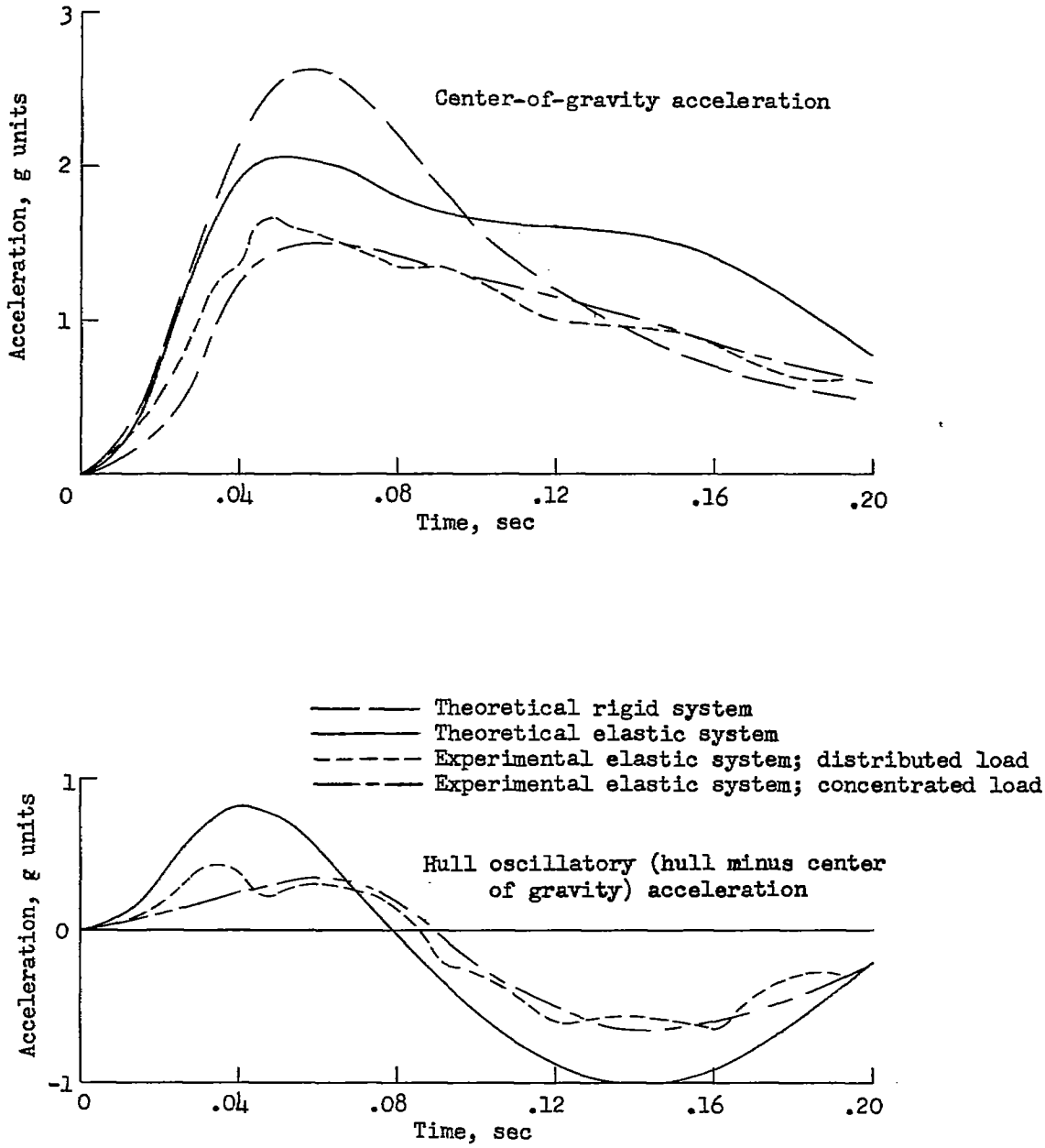

(b) Runs 13 and 14: $\tau = 3^{\circ}$; $\gamma \approx 14^{\circ}$; $V_0 \approx 34$ feet per second.

Figure 10.- Concluded.

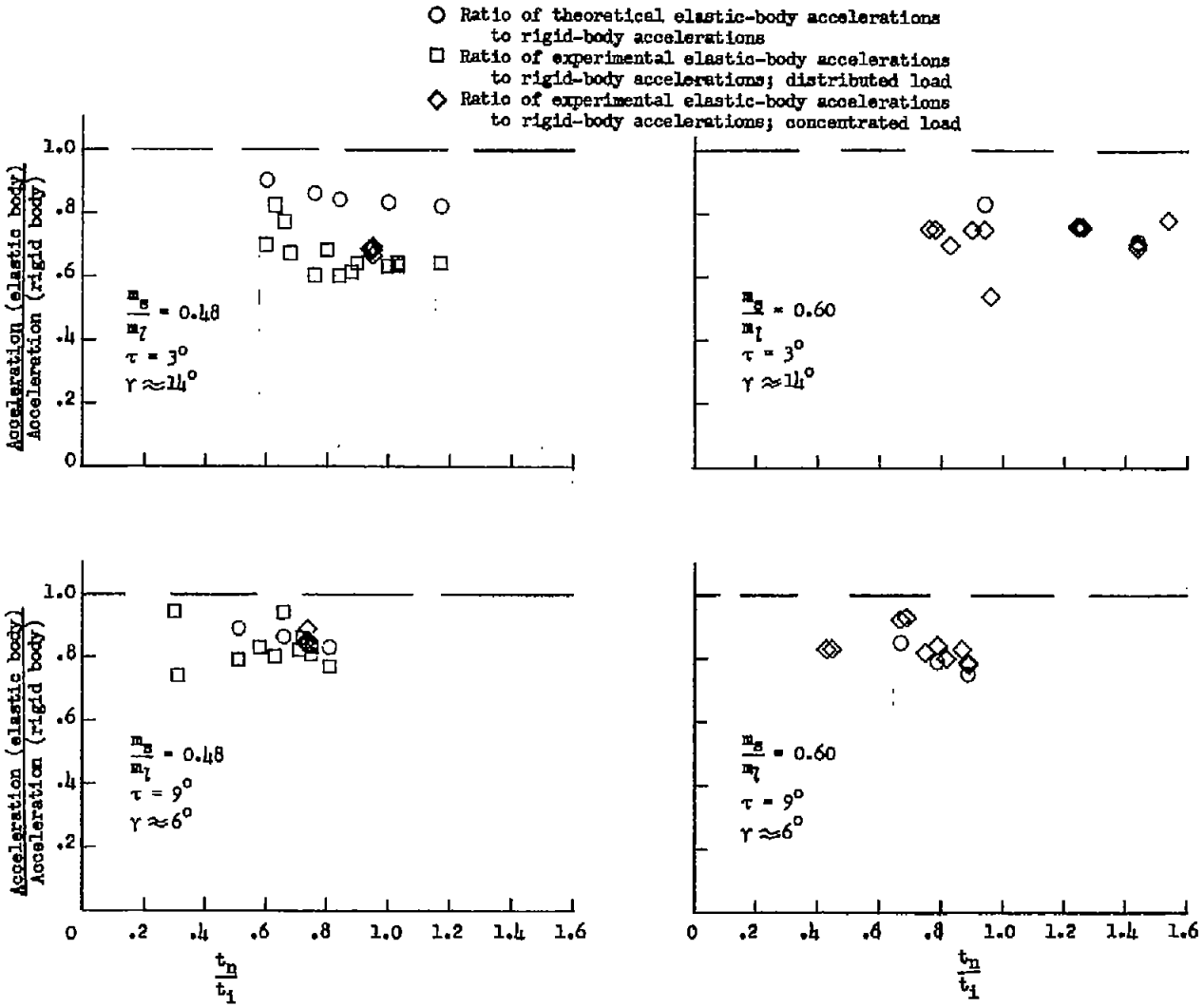

Figure 11.- Comparison of maximum theoretical and experimental hydrodynamic-impact accelerations expressed as the ratio of elastic-body acceleration to rigid-body acceleration.